View metadata, citation and similar papers at core.ac.uk
brought to you by CORE
provided by Brunel University Research Archive

Flow Patterns and Heat Transfer in a Square Cross-Section Micro Condenser Working at Low Mass Fluxes

Georges EL ACHKAR [1], Marc MISCEVIC [1*], Pascal LAVIEILLE [1], Jacques LLUC [1], Julien HUGON[2]

* Corresponding author: Tel: +33 561558307; Fax: +33 561556021; Email: marc.miscevic@laplace.univ-tlse.fr
[1] LAboratory PLAsma and Conversion of Energy (LAPLACE), Paul Sabatier University, Toulouse - France
[2] Thalès Alenia Space, Cannes - France

Abstract Flow patterns and heat transfer in an air-cooled square cross-section micro condenser were investigated. The test section consisted of a borosilicate square micro channel, of inner and outer hydraulic diameters of 0.49 mm and 0.6 mm respectively, and a length of 100 mm. The transparent material of the micro channel allowed the visualization of the different condensation flow patterns. The imposed mass velocities were ranging between 1 and 10 kg m^{-2} s^{-1}. In this range of mass fluxes, three main flow regimes were identified: Annular regime, intermittent regime, and spherical bubbles regime. Then, the isolated bubbles zone (the end of the intermittent zone + the spherical bubbles zone) was particularly studied. A specific experimental procedure was developed, basing on bubble tracking, in order to determine accurately the hydraulic and thermal parameters profiles in this zone according to the axial position in the micro channel, such as the vapour quality profile x(z). Thanks to energy balance, the liquid temperature profile $T_l(z)$ in the isolated bubbles zone was determined for different initial values. A thermal non-equilibrium between the liquid and vapour phases was identified. Therefore, the latent heat flux was then quantified and compared to the total heat flux in this zone.

Keywords: Two-Phase Flow, Condensation, Micro Channel, Square Cross Section, Flow Patterns, Heat Transfer

1. Introduction

The increase in the power dissipated in telecommunication satellites has gradually led to thermal control problems, which become now critical. In a long-term perspective and to anticipate on the future challenges, one solution is to increase the radiation temperature by the use of a cooling cycle of evaporation, compression, condensation, and expansion. The conditions under which operate condensers affect significantly performance and stability of these two-phase systems.

The gravitational field greatly influences the distribution of liquid and vapor in the condensers. In a space application context, it is important to operate in condition of low impact of the gravity. A possible solution is to reduce the size of the channels [1, 2]. Investigations available in literature are widely concentrated on flows with high mass velocities, of several hundreds of kg m^{-2} s^{-1} and particularly concerned condensation flow regimes, heat transfer, and pressure drops. For much lower range of mass velocities (i.e. several tens of kg m^{-2} s^{-1}), very few studies have been conducted. Three main flow regimes were identified for various diameters of the micro channel, channel shape and working fluids: the annular regime, the intermittent regime, and the spherical bubbles regime [2-8]. In previous works conducted in our laboratory, thermo-hydraulic characterization and modeling of the annular regime and of the spherical bubbles regime in a circular cross-section micro- condenser were performed [2, 8, 9, 10, 11].

The purpose of this paper is to propose a specific procedure to characterize the heat transfers in the isolated bubble zone, considering a square cross-section micro-condenser working at low mass fluxes. The procedure developed for this aim is first presented in details. Latent heat flux is then determined and compared to sensible heat flux for a mass velocity of 6.65 kg m^{-2} s^{-1}. Such a mass velocity is in the same order of magnitude than those encountered in thermal management systems such as loop heat pipes and capillary pumped loops.

2. Experiments

2.1 Experimental set-up

The main components of the experimental bench are an entrance tank, a temperature-controlled enclosure, a micrometric valve, the test section, a precision balance, a high-speed camera, an air-conditioning system, an exit tank and a data acquisition system (Fig. 1). Details of the setup are available in [11].

The entrance tank consisted of two coaxial cylinders. The internal one contained the n pentane as a working fluid (saturation temperature of 36 °C at atmospheric pressure) in both liquid and vapour phases. The saturation temperature is imposed thanks to thermostated water flowing in the annular space inside the tank. Hence, the inlet pressure was maintained constant throughout the experiments. The vapour was superheated in the temperature-controlled enclosure, which was set and maintained at sufficiently high temperature compared to the saturation temperature of the fluid, in order to prevent the condensation of the vapour upstream of the test section (in particular in the micrometric valve).

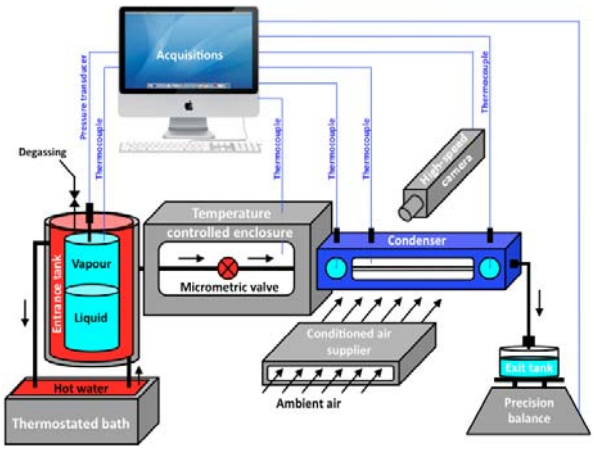

Figure 1: Schematic diagram of the experimental bench

Then, the vapour flowed in the test section, which consisted of a single borosilicate square micro channel, of 0.49 mm and 0.6 mm inner and outer hydraulic diameters respectively, and of 100 mm length, allowing the visualization of the condensation process through its transparent walls. To cool the external walls of the channel, a spot cooling air conditioning system was mounted perpendicularly to the test section in order to thermostated the air in the range 7 °C to 30 °C with an accuracy of 0.5 °C.

The mass flow rates of the n-pentane throughout the experiments were measured by weighing the condensates in the exit tank exposed to the ambient air (i.e. atmospheric pressure). Calibrated thermocouples allowed the temperatures measurements at several points of the working fluid circuits, with an accuracy of 0.2 °C, particularly in the inlet and outlet manifolds.

2.2 Experimental procedure

The outward heat transfer between the working fluid and the coolant mainly controls the condensation rate. Therefore, global heat transfer coefficient must be determined. The channel walls thickness was small enough to neglect the thermal conduction resistance. As the convective heat transfer between the air and the external walls of the channel was small compared to that within the channel, the global heat transfer coefficient can be identified as the external heat transfer coefficient.

In a previous study [11], a specific procedure using laser-induced fluorescence (LIF) was developed in order to determine this external convective heat transfer coefficient profile by measuring the temperature profile of liquid water when the test section was used as a liquid/air cross-flow heat exchanger. The same procedure was used again here.

2.3 Experimental campaigns

Before starting the experimental campaigns, the impurities and non-condensable gases in the n-pentane must be removed. In this aim, a specific degassing procedure was applied [11]. A high mass flow rate was imposed for few minutes in order to drive out the non-condensable particles from the circuits and to fill them with the working fluid. Then, a suitable mass flow rate was imposed in the test section by regulating the handle position of the micrometric valve.

The study of the isolated bubbles zone required the entire condensing process to occur

in the channel to be viewed. Therefore, the experiments were limited to mass velocities of 1.4, 2.9, 4.9, 6.65, and 8.77 kg m^{-2} s^{-1}. This low range of mass fluxes concerns several applications such as capillary pumped loops, loop heat pipes, or miniaturized loops.
For the results presented in this paper, the air conditioning system maintained the velocity and temperature of the airflow at approximately 8 m s^{-1} and 20 °C respectively throughout all the experiments. When the stability of the experimental conditions (e.g. mass flow rate, inlet and outlet temperatures of the test section, air temperature) was reached, a series of videos for the isolated bubbles zone was recorded, using the shadowgraph technique, using a high-speed camera mounted on a three dimensions adjustable trolley. The frame rates were 250 and 500 frames par second, chosen according to the bubbles detachment frequencies, and allowing an accurate detection of the bubbles kinetics. The lens magnification of the camera was determined as 99 pixel mm^{-1} with an accuracy of 1 pixel mm^{-1}. The acquisition windows consisted of 1024 columns of pixels corresponding thus to a real length of 10.34 mm. To cover the isolated bubbles zone length, the camera was moved along the axial position of the channel. A displacement of 7 mm was enough to see the total isolated bubbles zone length in two acquisition windows, and to keep a sufficient recovery zone.

3. Results and discussion

3.1 Flow patterns map

From a qualitative point of view, the flow structures in the square tube were similar to those obtained in previous studies conducted with a circular channel condenser [2, 8, 11, 12]. The condensation flow can be divided into three zones: the annular zone, the intermittent zone and the spherical bubbles zone (Fig. 2).
The transition between annular zone and intermittent zone may be attributed to instabilities appearing in the annular zone. Owing to the limiting heat transfer between the air and the external walls of the channel (i.e. the heat flux is small), the boiling number Bo (defined by the ratio of the outward heat flux to the heat flux released by phase change $h(T_{sat}-T_{air})/(G.l_v)$), representing almost the inverse of the two-phase zone length, was very small. Hence, the condensation zone length was many times greater than the smallest unstable wavelength $\lambda=4.D_{int}$ of the Rayleigh-Plateau instability [9].

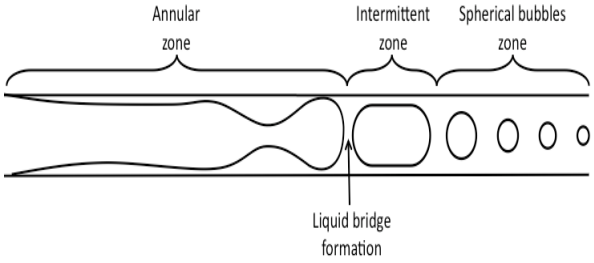

Figure 2: Condensation flow patterns

Two kinds of instability can be distinguished: convective instability and absolute instability [10]. The convective instability is characterized by the oscillations of the interface in the annular zone for a condensation length slightly higher than the unstable wavelength mentioned above. However, when the condensation length is widely greater than the unstable wavelength, a liquid bridge formation occurs, leading to the release of a bubble. This case corresponds to absolute instability, which is the case of the experiments presented in this paper. Consequently, for the conditions of cooling considered, the three flow patterns were always existed simultaneously.

3.2 Isolated bubbles zone

3.2.1 Treatment procedure

In order to determine the hydraulic and thermal flow parameters in the isolated bubbles zone, a specific procedure based on the Lagrangian tracking of the bubbles was developed. A specific Matlab program was realized to process the images of videos acquired using a high-speed camera.
In order to determine the real diameter of each bubble, the vapour location must first be determined. The developed program allows determining whether a white zone detected inside the channel corresponds to a liquid zone

(i.e. when it is close to the internal wall of the channel), and colored it in blue, or corresponds to a vapour zone and colored it in red (Fig. 3). It should be noted that the white cavities that belong to the walls were also colored in red even if there is no vapour. This does not modify the accuracy of the bubbles existence detection. Then, a local curve was determined for each image, indicating the presence or absence of a bubble along the channel length. This curve represented almost the void fraction $\alpha(z,t)$ in each cross-section, with an inaccuracy due to the under-estimated value of the internal hydraulic diameter of the channel determined by this procedure. A matrix can then be obtained, filled with 0 or 1 when the channel cross-section was totally or partially filled with liquid respectively.

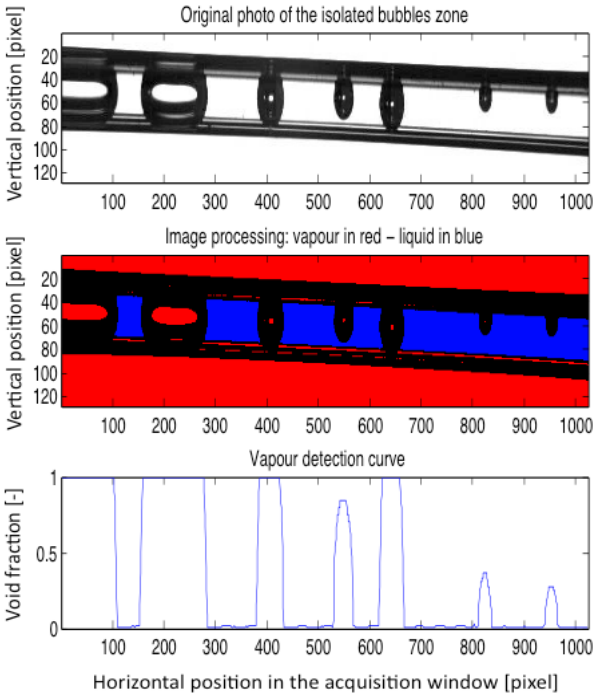

Figure 3: Example of the vapour presence indicator profile.

The row and column numbers of this matrix represented, respectively, the image number (i.e. time) and the position in the channel.
Once the matrix was filled, the total length of the channel was scanned backwards from the end to the beginning of the first row. The bubbles diameters and positions were then easily determined. A specific number was affected to each bubble. By iteration, the same procedure was applied to all the following rows. Moreover, the bubbles positions were compared between two successive images. If a bubble has moved below a arbitrary fixed number of pixels, the bubble keeps the same number in both of the images, else, the bubble get a new number (e.g. when bubbles enter the channel).
At the end of this step, two mains matrices were created: the first matrix contained the diameter evolution of each bubble number in function of the image number. The second matrix contained the evolution of the center position of the bubble in function of the image number.
In a second step, these two matrices were used together to determine the radius of all the bubbles that passed through each cross-section of the channel. To this end, the first cross-section was considered at the beginning of the channel (i.e. pixel number equals to 1), and it was shifted of one pixel by one pixel to reach the end of the channel (i.e. pixel number equals to 1024). Considering a given cross-section, the bubble numbers that passed by this cross-section were determined. Then, the diameter of each bubble was calculated by interpolating its two diameters at its nearest two positions before and after the considered cross-section. At the end of this step, another matrix was filled with the diameters of all the bubbles along the channel length (i.e. each row represented all bubbles diameters estimated in one cross-section).
As the discussion of the results was the same for the different mass velocities, only one example is reported, corresponding to a mass velocity G of 6.65 kg m^{-2} s^{-1}, illustrating the most important conclusions of this paper.

3.2.2 Determination of the hydraulic and thermal parameters

Knowing the spatial and temporal behaviour of each bubble radius 'R_b' during the overall time of the experiment Γ, the time averaged vapour quality in any cross-section of the channel along the isolated bubbles zone can be determined:

$$x = \frac{\rho_v}{\Gamma \dot{m}} \sum_{i=1}^{N} V_{b,i}$$

where $V_{b,i}$ is the volume of the bubble i.

Owing to the instability mentioned previously, the spherical bubbles zone fluctuated. A zone where the spherical and elongated bubbles alternatively exist was observed (Fig. 4). In addition, at the beginning of the acquisition window, the bubbles entering the channel were not seen as complete bubbles (the left part of the bubbles is outside the acquisition window). So, determinations of the beginning of isolated bubbles zone must be define. We considered the beginning of this zone to be at the position where only 5 % of the bubbles were incomplete.

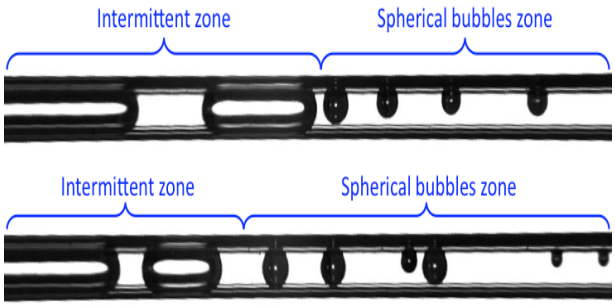

Figure 4: Example of the fluctuation of the spherical bubbles zone during time for G=6.65 kg m^{-2} s^{-1}.

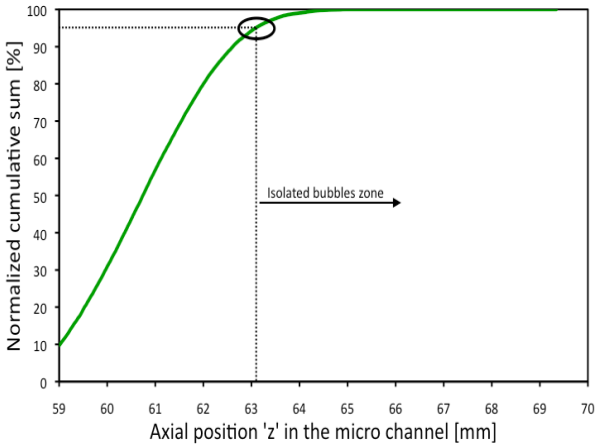

Figure 5: Evolution of the cumulative sum of the incomplete bubbles end in the first acquisition window for G=6.65 kg m^{-2} s^{-1}.

Figure 5 shows the normalized cumulative sum of the end positions of the incomplete bubbles in the first acquisition window. The entrance position of the isolated bubbles zone was then found to be 63.1 mm. However, this zone always contained elongated bubbles. The region where all the bubbles had a spherical shape was considered to begin at the position beyond which all the bubbles diameters are smaller than the internal hydraulic diameter of the channel.

The figure 6 shows two quality profiles: the first was determined when all the bubbles were taken into consideration (blue line), and the second was determined when only spherical bubbles were considered (red line). The parts of the two profiles where the vapour volumes of the incomplete bubbles could not be calculated were not plotted in this figure. The 2 plain vertical lines indicate the beginnings of the isolated bubbles zone and of the spherical bubbles zone respectively (according to the definitions previously indicated).

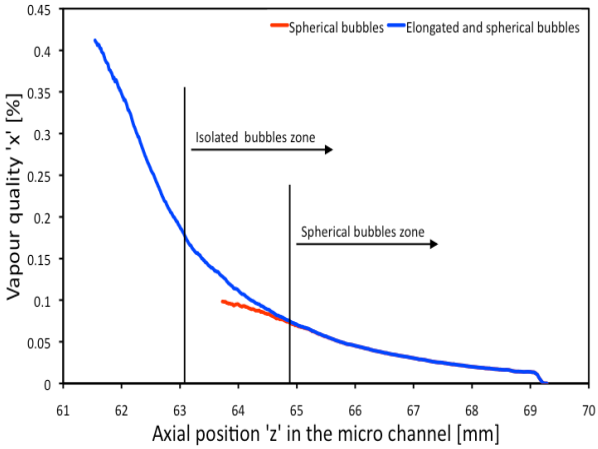

Figure 6: Average quality evolutions in the first acquisition window of the bubbles zone for G=6.65 kg m^{-2} s^{-1}: the blue line represents the quality evolution calculated with both elongated and spherical bubbles; the red line represents the quality evolution taking into account only spherical bubbles.

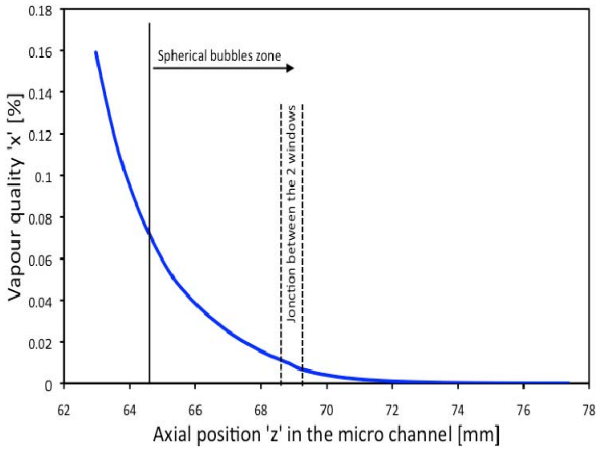

Figure 7: Average quality evolution x(z) in the isolated bubbles zone for G=6.65 kg m^{-2} s^{-1}.

The vapour quality profile is plotted in the figure 7 for the isolated bubbles zone. The

order of magnitude of this vapour quality is very low (< 0.2 %), indicating that phase change was mainly occurred upstream of this zone (i.e. in the annular and intermittent zones). It should be noticed that the thermodynamic vapour quality is even lower than this one.

Considering the limiting aspect of the external heat transfer due to air-cooling process, and supposing the liquid phase to be at the saturated temperature, the quality profile should be almost linear (considering low spatial variations of the external heat transfer coefficient). However, the quality evolution was not linear, as can be seen in the figure 7. Such behavior indicates thermal non-equilibrium between the liquid phase (that should be subcooled) and the vapour phase (at the saturation temperature). Hence, the role of the sensible heat transfer appears to be not nil in this zone and can be deduced from the energy balance.

Regardless of the low rate of phase change in the isolated bubbles zone in comparison with the upstream zones, it can be noted that the vapour quality gradient is greater at the beginning (i.e. about 30 % of the total zone length) of this zone than in the remaining part, reflecting a great released part of the latent heat in comparison with the remaining zone length. Indeed, during condensation process, the bubble interface and the thermal diffusion move in opposite directions, increasing the thermal boundary layer thickness until the complete condensation of the bubble. This process decreases the conductive heat transfer density between the bubble and the surrounding subcooled liquid [13-15].

The time averaged energy balance equation governing this type of flow is given by:

$$\frac{\dot{m}_l}{A} C_{pl} \frac{dT_l(z)}{dz} + \frac{\dot{m} l_v}{A} \frac{dx}{dz} = 4h_g \frac{D_{ext}}{D_{\text{int}}^2} \left(T_{air} - T_l(z)\right)$$

Where h_g is the global heat transfer coefficient between the working fluid and the coolant. As the external heat transfer is limiting, the global heat transfer coefficient is almost equal to the external heat transfer coefficient ($h_g \approx h_{ext}$) determined by the LIF method as mentioned previously.

Applying the energy balance equation turns out the liquid temperature profile in the isolated bubbles zone. However, the initial value of the temperature at the beginning of the isolated bubbles zone was not yet known because of the unknown heat transfers occurring in the intermittent zone. So, several initial values of entrance temperature were imposed in order to show their impact on the distribution of the heat transfers (sensible or latent) existing in this zone. The profiles are shown in the figure 8. It should be noted that the entrance temperature could not be determined by imposing the outlet temperature, which was measured at a distance of 1 cm from the channel outlet.

The figure 8 shows that whatever the entrance temperature of liquid is, the decrease of the liquid temperature along the isolated bubbles zone was significant (e.g. about 10 °C for an entrance temperature of 36 °C). Therefore, the hypothesis of a single temperature zone (i.e. saturated temperature) is no longer valid for such a condensation flow.

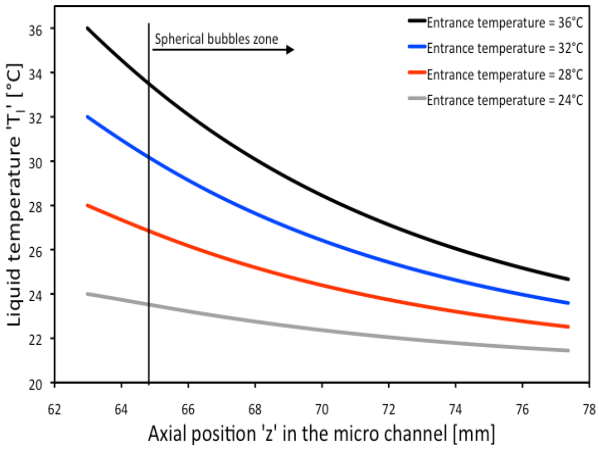

Figure 8: Liquid temperature evolutions $T_l(z, T_0)$ in the isolated bubbles zone for G=6.65 kg m^{-2} s^{-1}.

The impact of this temperature variation on the distribution of the latent and sensible heat transfer is represented in figure 9. This figure shows the percentage of the latent heat transfer released in the isolated bubbles zone compared to the total heat released.

The profiles showed that the heat flux dissipated by phase change at the origin of the isolated bubbles zone represents almost 35 % of the total heat flux in the worst case (i.e. for

an entrance liquid temperature of 24 °C). This proportion decreases rapidly during bubble condensation. Beyond a position of about 20 to 30 % of the total zone length, the latent heat flux becomes minor, representing less than 10 % of the total heat flux. By averaging the latent heat transfer along the total length of the isolated bubbles zone, a maximum value of 6 % was found in the worst cases.

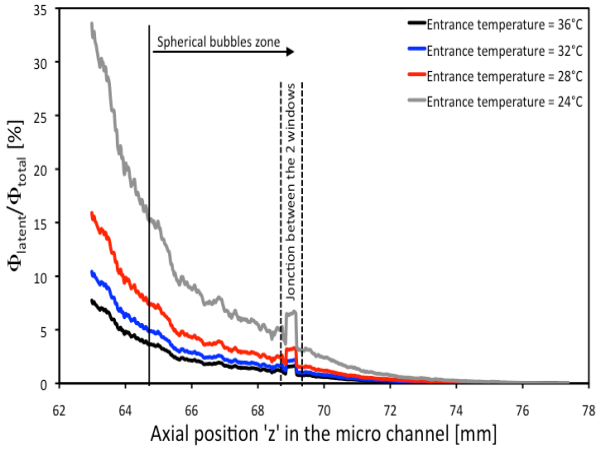

Figure 9: Ratio evolutions of the latent heat transfer form released to the total heat released in the isolated bubbles zone for G=6.65 kg m^{-2} s^{-1}.

Consequently, from heat transfer point of view, this zone may be considered as a single-phase (liquid phase) zone for the condensers design.
Significant discrepancies were detected in the profiles of figure 9, between the two positions 68.5 and 69.5 mm of the channel. This resulted from the recovery of the different quality profiles of the two acquisition windows (affecting the quality gradient profile and thus the latent heat profile).

Conclusions

The condensation flow in an air-cooled square cross-section micro condenser, working at mass fluxes in the order of magnitude of 10 kg m^{-2} s^{-1}, can be divided into three main zones: the annular zone, the intermittent zone and the spherical bubbles zone. Physical definitions were given to the isolated bubbles and spherical bubbles zones, allowing the determination of the beginnings of these two zones. A specific experimental procedure, basing on bubble tracking, was developed and detailed. It allowed the determination of the hydraulic and thermal parameters profiles in this zone such as the average local quality profile x(z), the average liquid temperature profile $T_l(z)$, and the ratio profile of the latent heat flux to the total heat flux $\Phi_{latent}(z)/\Phi_{total}(z)$. The results showed that the magnitude of the quality was very small (less than 0.2 %), implying negligible latent heat flux in the isolated bubbles zone in comparison with the annular and the intermittent zones. The non-negligible liquid temperature variation in this zone highlighted the thermal non-equilibrium between the liquid and the vapour phases. The evolution of the latent heat flux with respect to the total heat flux showed that a mean value of less than 6 % of the heat transfer was in latent form in the isolated bubbles zone, for the lowest (i.e. worst) initial temperature hypothesis. So, from a thermal point of view, this zone can be considered as a single liquid phase zone.

Outlook

The determination of the real entrance temperature of the isolated bubbles zone should be determined. Therefore, the intermittent zone has to be well investigated. A further study with larger range of mass velocities must be conducted in order to find out the heat transfer laws and correlations.

Acknowledgements

Financial supports from FNRAE (MATRAS) and from the Microgravity Application Program of the European Space Agency are gratefully acknowledged.

Nomenclature

A	cross-section area of the tube	m^2
Bo	boiling number	—
c_p	specific heat	J kg^{-1} K
D	hydraulic diameter	m
G	mass velocity	kg m^{-2} s^{-1}
h	heat transfer coefficient	W m^{-2} K^{-1}
i	variable	—
l_v	latent heat of vaporization	J kg^{-1}

m	mass flow rate	kg s^{-1}
N	total number of bubbles	—
R	radius	m
t	time	s
T	temperature	°C
U	velocity	m s^{-1}
V	volume	m^3
x	vapour quality	—
z	axial position of the channel	m

Greek symbols

ρ	density	kg m^{-3}
λ	instability wave length	m
α	void fraction	—
Γ	total duration of the experiment	s

Subscripts

b	bubble
ext	external
g	global
int	internal
l	liquid
sat	saturation
v	vapour

References

[1] S. Nebuloni, J.R. Thome, Numerical modeling of laminar annular film condensation for different channel shapes. International Journal of Heat and Mass Transfer 53 (2010) 2615-2627

[2] B. Médéric, M. Miscevic, V. Platel, P. Lavieille, J.L. Joly, Experimental study of flow characteristics during condensation in narrow channels: influence of diameter channel on structure patterns, Superlattices Microstruct. 35 (2004) 573-586.

[3] J.W. Coleman, S. Garimella, Two-phase flow regimes in round, square and rectangular tubes during condensation of refrigerant R134a, Int. J Refrigeration 26 (2003) 117-128.

[4] J. El Hajal, J.R. Thome, A. Cavallini, Condensation in horizontal tubes, part 1: two-phase flow pattern map, Int. J. Heat Mass Transfer 46 (2003) 3349-3363.

[5] H.Y. Wu, P. Cheng, Condensation flow patterns in silicon microchannels, Int. J. Heat Mass Transfer 48 (11) (2005) 2186-2197.

[6] J.S. Hu, C. Y.H. Chao, An experimental study of the fluid flow and heat transfer characteristics in micro-condensers with slug-bubbly flow, Int. J. Refrigeration 26 (2007) 117-128.

[7] H. Louahlia-Gualous, B. Mecheri, Unsteady steam condensation flow patterns inside a miniature tube, Applied Thermal Engineering 27 (2007) 1225-1235.

[8] B. Médéric, P. Lavieille, M. Miscevic, Heat transfer analysis according to condensation flow structures in a minichannel, Exp. Thermal Fluid Sci. 30 (2005) 785-793.

[9] M. Miscevic, P. Lavieille, B. Piaud, Numerical study of convective flow with condensation of a pure fluid in capillary regime, Int. J. Heat Mass Transfer 52 (2009) 5130-5140.

[10] B. Piaud, P. Lavieille, M. Miscevic, About stability of a vapour jet condensing in a micro channel, in: International Heat Transfer Conference (IHTC14), Washington, DC, USA, 2010, pp. 22862.

[11] G. El Achkar, P. Lavieille, J. Lluc, M. Miscevic, Heat transfer and flow distribution in a multichannel microcondenser working at low mass fluxes, Int. J. Heat Mass Transfer 54 (2011) 2319-2325.

[12] B. Médéric, P. Lavieille, M. Miscevic, Void fraction invariance property of complete condensation flow inside a capillary glass tube, International Journal of Multiphase Flow 9 (2005) 1049-1056.

[13] L.W. Florschuetz, B.T. Chao, On the mechanics of vapor bubble collapse, Int. J. Heat Mass Transfer Trans.ASME 87 (1965) 209-220.

[14] A. D. Okhotsimskii, The thermal regime of vapour bubble collapse at different Jacob numbers, Int. J. Heat Mass Transfer 31 (1988) 1569-1576.

[15] D. Legendre, J. Boree, J. Magnaudet, Thermal and dynamic evolution of a spherical bubble moving steadily in a superheated or subcooled liquid, Phys. of Fluid 10 (1998) 1256-1272.